Contributions to Mineralogy and Petrology (2024) 179:6
https://doi.org/10.1007/s00410-023-02085-x

ORIGINAL PAPER

Titanium isotopic fractionation during alkaline magma differentiation at St. Helena Island

Xinmiao Zhao[1,2] · Xiao-Jun Wang[3] · Xiliang Jia[1,4] · Noreen J. Evans[5] · Chunxia Yi[1,4] · Li-Hui Chen[3] · Takeshi Hanyu[6] · Jin Li[7] · Bo Wan[1,2] · Xiangkun Zhu[7] · Hongfu Zhang[8]

Received: 18 June 2023 / Accepted: 23 November 2023 / Published online: 27 December 2023

Abstract

To better understand the behavior of Ti isotope fractionation during alkaline magma differentiation, we studied well characterized alkaline lavas from St. Helena Island (South Atlantic), as well as their titanomagnetite separates. The lavas are classified into three groups according to petrographic observations and major element composition. Group 1 and Group 2 samples (5 to > 13 wt.% MgO) have a narrow $\delta^{49/47}$Ti range (− 0.02 to 0.05‰), suggesting that Ti isotopic fractionation is insignificant in less evolved basaltic lavas. Conversely, Group 3 samples (MgO < 5 wt.%) are saturated with titanomagnetite and display a wide range in $\delta^{49/47}$Ti (− 0.02 to 1.96‰). The $\delta^{49/47}$Ti values for Group 3 samples show significant correlation with TiO_2 and SiO_2 content, as well as with Mg and Fe isotopic values. Moreover, titanomagnetite phenocrysts from Group 3 rocks have remarkably lighter $\delta^{49/47}$Ti values (− 0.54 to 0.01‰) relative to the corresponding whole rock (− 0.02 to 0.21‰), indicating that titanomagnetite crystallization exerts significant control over the $\delta^{49/47}$Ti of Group 3 samples. These observations are further supported by modeling calculations. Together with published Ti isotope data, the results demonstrate that the range in Ti isotopic evolution in alkaline, calc-alkaline and tholeiitic magmatic systems is controlled by fractional crystallization of diverse Fe-Ti oxides with contrasting Ti isotopic compositions. This makes Ti stable isotopes an important geochemical tracer for magma evolution.

Keywords Ti isotopes · Isotope fractionation · Alkaline magma differentiation · Fe–Ti oxides · St. Helena Island

Introduction

Titanium is a moderately incompatible element in magmatic systems and becomes concentrated in crustal rocks relative to the mantle. It has five stable isotopes (^{46}Ti, ^{47}Ti, ^{48}Ti, ^{49}Ti and ^{50}Ti) and its isotopic variations have been increasingly used to probe numerous fundamental geochemical and cosmochemical processes such as planetary differentiation, crust production and crust-mantle interaction (e.g., Millet et al. 2016; Greber et al. 2017a, 2017b, 2021; Deng et al. 2018a, 2018b, 2019, 2023; Mandl 2019; Johnson et al. 2019, 2023; Aarons et al. 2020; Kommescher et al. 2020; Zhao et al. 2020; Hoare et al. 2020, 2022; Rzehak et al. 2021, 2022; Williams et al. 2021; Anguelova et al. 2022; Storck et al. 2023). Early studies demonstrated that Fe-Ti oxide unsaturated

Communicated by Othmar Müntener.

✉ Xinmiao Zhao
xinmiao312@mail.iggcas.ac.cn

1 State Key Laboratory of Lithospheric Evolution, Institute of Geology and Geophysics, Chinese Academy of Sciences, Beijing 100029, China

2 Innovation Academy of Earth Science, Chinese Academy of Sciences, Beijing, China

3 State Key Laboratory of Continental Dynamics, Department of Geology, Northwest University, Xi'an 710069, China

4 University of Chinese Academy of Sciences, Beijing, China

5 John de Laeter Centre, Curtin University, Perth, WA 6945, Australia

6 Japan Agency for Marine-Earth Science and Technology, Research Institute for Marine Geodynamics, Yokosuka 237-0061, Japan

7 MLR Key Laboratory of Isotope Geology, Institute of Geology, Chinese Academy of Geological Sciences, Beijing 100037, China

8 School of Earth Sciences, Zhejiang University, Hangzhou 310027, China

terrestrial mafic and ultramafic rocks such as komatiites and global oceanic basalts display limited Ti isotopic variation ($\delta^{49/47}$Ti between −0.05 and 0.05 ‰), although a small, but resolvable Ti isotopic variation has been observed in komatiites and mid-ocean ridge basalts (Millet et al. 2016; Greber et al. 2017a; Deng et al. 2018b; Zhao et al. 2020). By contrast, differentiated igneous rocks display systematically heavier Ti isotopic compositions that correlate with indicators of magmatic differentiation such as SiO_2 or MgO contents, which is assumed to be primarily controlled by saturation and fractionation of isotopically light Fe-Ti oxides during magmatic differentiation (Millet et al. 2016; Greber et al. 2017a). These findings make Ti isotopes a promising tracer of diverse geological and cosmochemical processes. However, subsequent work has demonstrated that the Ti isotope behavior becomes more complicated during magmatic differentiation, and different magmatic systems (such as alkaline, tholeiitic and calc-alkaline) exhibit different Ti isotopic evolution patterns (Millet et al. 2016; Deng et al. 2019; Johnson et al. 2019; 2023; Zhao et al. 2020; Hoare et al. 2020, 2022; Aarons et al. 2021; Greber et al. 2021; Storck et al. 2023). For example, alkaline magmatic series have significantly higher $\delta^{49/47}$Ti (exceeding 2‰) relative to subduction-related systems such as calc-alkaline magmatism and arc tholeiites (up to 0.7‰) at the same SiO_2 content, likely related to the much higher initial melt TiO_2 contents enabling early saturation and fractional crystallization of Fe-Ti oxide with higher TiO_2 contents in the alkaline magmatic series than subduction zone lavas (Deng et al. 2019; Johnson et al. 2019; 2023; Aarons et al. 2020, 2021; Hoare et al. 2020, 2022). Such distinct Ti isotope evolution patterns in igneous systems have led to controversial conclusions on the geodynamic origin of felsic continental crust (Greber et al. 2017b; Deng et al. 2019; Aarons et al. 2020, 2021). Further studies are required to investigate the cause of these complex Ti isotope variations in different magmatic systems.

St. Helena Island (5° 40′W, 16° 00′S), in the South Atlantic, provides us with a natural laboratory in which to investigate the impact of alkaline magma differentiation on Ti isotopes. These lavas experienced fractional crystallization and mineral accumulation processes from a cogenetic mantle source, as deduced from their major and trace element chemistry, and radiogenic isotope characteristics (Baker 1969; Kawabata et al. 2011; Hanyu et al. 2014). This study investigates the Ti isotopic systematics of a well-characterized St. Helena alkaline sample suite (Kawabata et al. 2011; Hanyu et al. 2014; Wang et al. 2021; Zhao et al. 2022). Combined with published Ti isotopic ratios for other igneous rocks, we aim to further explore the origin of Ti isotope variation in different magmatic systems.

Samples and analytical methods

The studied alkaline lavas were collected from St. Helena Island in the middle of the South Atlantic (Chaffey et al. 1989; Kawabata et al. 2011). Twenty-four samples, covering basanite-alkali basalt, trachyandesite and trachyte, along with three hand-picked titanomagnetite separates from St. Helena Island were selected for Ti isotopes analyses. They have previously been studied for petrology, major and trace element composition, and radiogenic/stable isotopic composition, and their magmatic evolution has been well characterized (Kawabata et al. 2011; Hanyu et al. 2014; Wang et al. 2021; Zhao et al. 2022; Zhang et al. 2022). These samples span a range of SiO_2 contents from 43.5 to 61.4 wt.%, MgO contents from 0.05 to 15.7 wt.%, total-alkali ($Na_2O + K_2O$) contents from 1.7 to 12.6 wt.%, and TiO_2 contents from 0.11 to 3.86 wt.% (Fig. 1; Kawabata et al. 2011; Table S1 in Supporting Information S1). They can be classified into three groups according to their petrological and geochemical features (Kawabata et al. 2011). Group 1 samples (MgO content > 13 wt.%) contain a substantial amount of cumulate olivine and clinopyroxene (Fig. 1). Group 2 samples (MgO content; 5 wt.% to 12 wt.%) experienced olivine and clinopyroxene crystallization (Fig. 1; Kawabata et al. 2011). Group 3 samples (MgO content < 5 wt.%) experienced massive fractionation of plagioclase and Fe-Ti oxide, with minor amounts of apatite, olivine and clinopyroxene (Fig. 1; Kawabata et al. 2011). In Group 3 samples, Fe-Ti oxide (titanomagnetite) crystallized and fractionated as evidenced by the appearance of this phase (Wang et al. 2021; Zhao et al. 2022), and the clear decrease in TiO_2 and FeO_T contents at the 5 wt.% MgO inflection on whole rock diagrams (Fig. 1; Kawabata et al. 2011). Based on detailed scanning electron microscope (SEM) backscattered electron (BSE) images, energy-dispersive spectroscopy (EDS) spectra, and electro-probe microanalyzer data, Wang et al. (2021) and Zhao et al. (2022) have shown that all the Fe-Ti oxide phenocrysts from St. Helena lavas are ulvöspinel-rich titanomagnetite. SEM images also show that titanomagnetite phenocrysts in Group 3 samples are generally in contact with groundmass and devoid of exsolution lamellae of other Fe-Ti oxides, indicating they are equilibrium with the melt. The ulvöspinel-rich titanomagnetite separates analyzed from the three Group 3 samples (SH-62, SH-17, SH-89) were initially separated using Frantz magnetic selection, and then were hand-picked under a binocular microscope. The ulvöspinel-rich titanomagnetite separates in every sample show narrow chemical variations with TiO_2 contents ranging from 18.7–22.7 wt.%, FeO_T contents ranging from 65.5−69.9 wt.%, and low contents of MgO (2.45−4.68 wt.%) and SiO_2 (0.04–0.12

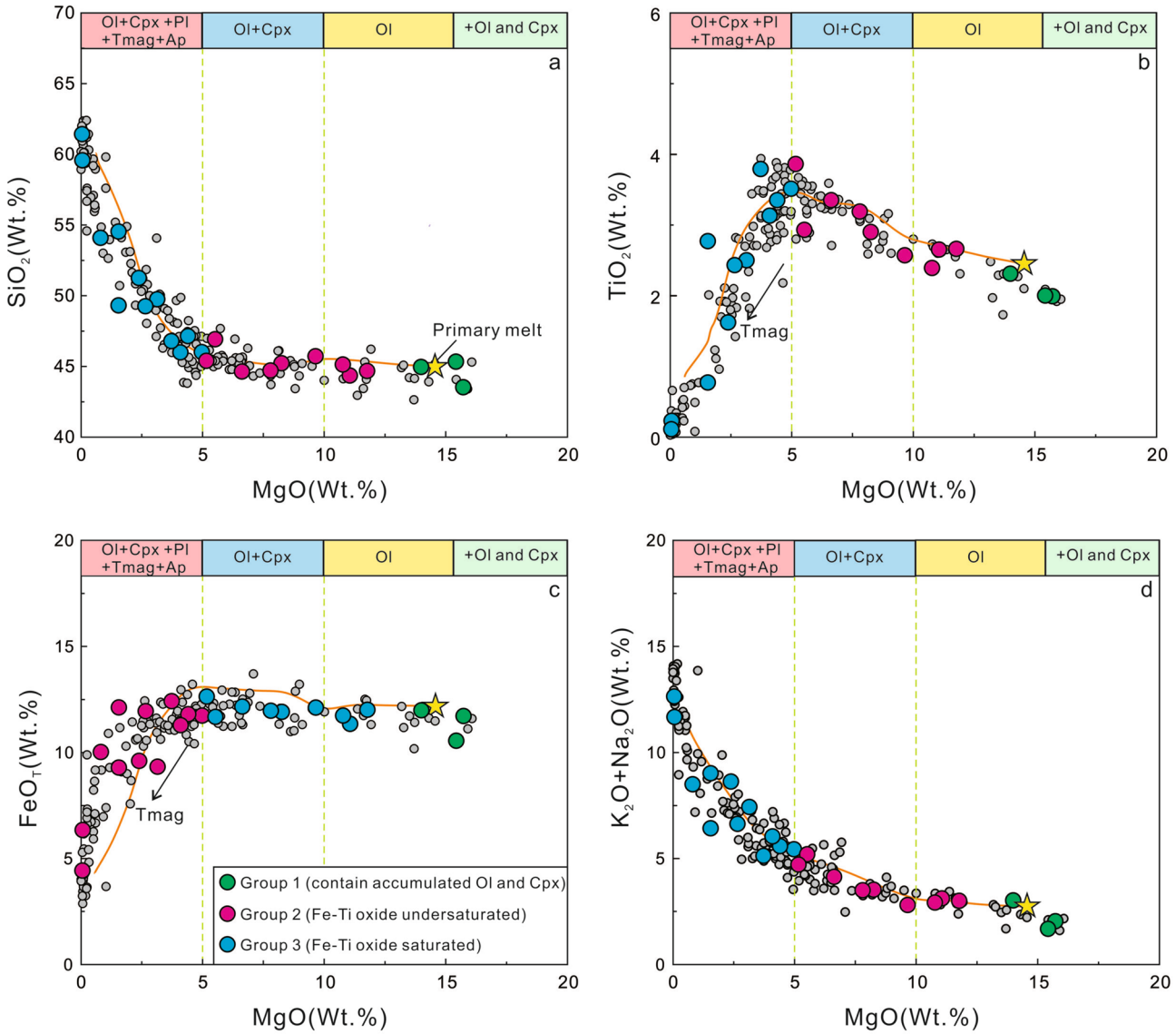

Fig. 1 Magmatic differentiation in the St. Helena lavas illustrated by **a** SiO_2, **b** TiO_2, **c** FeO_T (total iron as FeO) and **d** Na_2O+K_2O contents as a function of MgO contents. The major element data and the composition of primary melt are from Kawabata et al. (2011) and are also available in Table S1 of Supporting Information S1. Orange lines represent the MELTS-calculated fractional crystallization paths of St. Helena lavas with initial oxygen fugacity of QFM + 1 and a constant pressure of 3 kbar (see Sect. 5.1 of Wang et al. (2021) for more information). All published data (small gray circles) for St. Helena rock samples are also shown for comparison, which are collected from GEOROC (http://georoc.mpch-mainz.gwdg.de/georoc/) database, and can be found in the Table S2 of Supporting Information S1 with detailed references. *Ol* olivine, *Cpx* clinopyroxene, *Pl* plagioclase, *Tmag* titanomagnetite, Ap apatite

wt.%) (Table 1; Wang et al. 2021; Zhao et al. 2022). More information about these volcanic rocks can be found in the literature (Baker 1968; Kawabata et al. 2011; Hanyu et al. 2014; Wang et al. 2021; Zhao et al. 2022).

Chemical separation and Ti isotope measurements were carried out at the Laboratory of Isotopic Geology, Institute of Geology, Chinese Academy of Geological Sciences, Beijing, China, following the methods outlined in Zhao et al. (2020) and Li et al. (2022). Details of the Ti isotope analytical methods are given in Supporting Information S2. Titanium isotope data are presented as δ values in per mil relative to the OL-Ti standard: $\delta^{49/47}Ti\ (‰) = [(^{49}Ti/^{47}Ti)_{sample}/(^{49}Ti/^{47}Ti)_{OL\text{-}Ti} - 1] \times 1000$. The long-term average $\delta^{49/47}Ti$ of NIST3162a and IGPG-Ti are $1.06 \pm 0.04‰$ (n = 173, 2SD) and $0.14 \pm 0.03‰$ (N = 42, 2SD), respectively (Table 1), consistent with published data (Greber et al. 2017a; Deng et al. 2018a; Zhao et al. 2020; Li et al. 2022). In addition, the $\delta^{49/47}Ti$ values of BHVO-2, AGV-1 and GSP-2 obtained during this study agree well with previous works (Table 1; Millet and Dauphas 2014; Millet et al. 2016; Greber et al.

Table 1 Ti isotopic composition and selected major element data of alkaline volcanic rock samples from St. Helena Island

Sample	Lithology	Group	$\delta^{49/47}$Ti	2SD	N[a]	SiO_2[b]	TiO_2	MgO	Na_2O+K_2O
SH-35	Picritic basalt	Group1	0.03	0.03	3	43.52	1.99	15.72	2.03
SH-86	Basalt	Group1	0.03	0.03	3	45.33	2.00	15.42	1.67
SH-25	Basalt	Group1	0.04	0.02	3	44.95	2.31	13.99	3.01
SH-84	Basalt	Group2	0.04	0.03	3	44.67	2.66	11.77	2.99
SH-45	Basalt	Group2	0.00	0.03	3	44.35	2.65	11.06	3.11
SH-38	Basalt	Group2	0.05	0.03	3	45.12	2.39	10.77	2.91
SH-15	Basalt	Group2	0.02	0.04	3	45.71	2.57	9.65	2.80
SH-10	Basalt	Group2	0.05	0.02	3	45.22	2.90	8.25	3.52
SH-50	Basalt	Group2	0.00	0.02	3	44.70	3.19	7.80	3.49
SH-109	Basalt	Group2	0.03	0.02	3	44.63	3.35	6.62	4.12
SH-99	Trachybasalt	Group2	0.05	0.04	3	46.91	2.93	5.52	5.19
SH-12	Basalt	Group2	−0.02	0.02	3	45.39	3.86	5.16	4.70
SH-58	Trachybasalt	Group3	0.05	0.02	3	46.00	3.51	4.97	5.42
SH-76	Trachybasalt	Group3	0.09	0.03	3	47.13	3.35	4.40	5.57
SH-62	Trachybasalt	Group3	0.14	0.04	3	45.98	3.13	4.09	6.03
SH-17	Trachybasalt	Group3	−0.02	0.03	3	46.78	3.79	3.72	5.11
SH-73	Trachybasalt	Group3	0.25	0.03	3	49.74	2.50	3.14	7.42
SH-89	Trachybasalt	Group3	0.21	0.04	3	49.24	2.43	2.65	6.62
SH-43	Trachybasalt	Group3	0.15	0.03	3	49.30	2.77	1.55	6.41
SH-59	Trachybasalt	Group3	0.41	0.04	3	51.24	1.62	2.38	8.62
SH-53	Trachybasalt	Group3	0.69	0.02	3	54.53	0.77	1.55	9.01
SH-93	Trachybasalt	Group3	0.34	0.04	3	54.08	1.22	0.81	8.49
SH-30	Trachybasalt	Group3	1.58	0.02	3	59.56	0.23	0.06	11.66
Replicate[c]	Trachybasalt	Group3	1.61	0.03	3	59.56	0.23	0.06	11.66
SH-42	Trachybasalt	Group3	1.96	0.04	3	61.41	0.11	0.05	12.63
SH-17	Titanomagnetite	Group3	−0.43	0.03	3	0.09	21.3	3.73	0.03
Replicate			−0.45	0.02	3	0.09	21.3	3.73	0.03
SH-89	Titanomagnetite	Group3	0.01	0.02	3	0.10	21.4	4.23	0.02
Replicate			−0.01	0.02	3	0.10	21.4	4.23	0.02
SH-62	Titanomagnetite	Group3	−0.53	0.03	3	0.06	21.0	2.67	0.02
Replicate			−0.54	0.02	3	0.06	21.0	2.67	0.02
Reference materials									
SRM3162a			1.06	0.04	173				
IPGP-Ti			0.14	0.03	42				
BHVO-2			0.02	0.03	6				
AGV-1			0.09	0.03	6				
GSP-2			0.38	0.03	4				

[a]N is the number of repeat measurements of the purified Ti solution;

[b]Data for SiO_2, MgO, TiO_2, Na_2O and K_2O are from Kawabata et al. (2011)

[c]Replicate represents the repeat sample dissolution, column chemistry and instrumental analysis

2017a, 2017b, 2021; Deng et al. 2018a, 2018b, 2019; Johnson et al. 2019; Mandl 2019; Zhao et al. 2020; He et al. 2020; Hoare et al. 2020, 2022; Li et al. 2022). Replicates of four samples (SH-30, and titanomagnetite phenocrysts of SH-17, SH-89 and SH-62), which were digested from different aliquots of sample powder, display identical results within uncertainty (Table 1).

Samples SH-30 and SH-42 were also analyzed for Fe isotopes to complement the existing dataset. These measurements were carried out on a Thermo Scientific Neptune Plus multi-collector inductively coupled plasma

mass-spectrometer (MC-ICPMS) at the State Key Laboratory of Continental Dynamics of Northwest University, China, using the sample-standard bracketing method under "wet" plasma conditions (Chen et al. 2022). Details of the Fe isotope analytical methods are provided in Supporting Information S2. Each sample was measured a minimum of three times. The Fe isotope data are reported using δ notation against the IRMM-014 standard: $\delta^{X/54}Fe$ (‰) = $[(^{X}Fe/^{54}Fe)_{sample}/(^{X}Fe/^{54}Fe)_{IRMM\text{-}014} - 1] \times 1000$, where X refers to 57 or 56. The long-term reproducibility for $\delta^{57/54}Fe$ data is better than 0.07‰ (2SD; Table S3 in Supporting Information S1). Reference materials BCR-2 and BHVO-2 were analyzed with samples, giving $\delta^{57/54}Fe$ values similar to published values (Table S3 in Supporting Information S1; Craddock and Dauphas 2011; Sossi et al. 2012; Zhao et al. 2012; He et al. 2015; Konter et al. 2016; An et al. 2017; Zhao et al. 2022) when the equivalent 2 SD errors are considered.

Results

Titanium isotopic data for the St. Helena lavas are shown in Table 1, along with other geochemical data. The St. Helena whole-rock samples display large Ti isotopic variations with $\delta^{49/47}Ti$ ranging from −0.02 to 1.96‰ (Fig. 2 and Table 1). Specifically, samples from Group 1 and Group 2 (MgO > 5 wt.%) show insignificant $\delta^{49/47}Ti$ variation (−0.02–0.05‰), regardless of their chemical composition (e.g., SiO_2, TiO_2, MgO or $Na_2O + K_2O$ composition; Fig. 2 and Table 1), which agrees well with the limited range in $\delta^{49/47}Ti$ reported for global oceanic basalts and komatiites (Millet et al. 2016; Greber et al. 2017a; Deng et al. 2018a, 2019, 2023; Zhao et al. 2020). Compared with the other two groups, Group 3 samples show a remarkable $\delta^{49/47}Ti$ variation (from −0.02 to 1.96‰ for $\delta^{49/47}Ti$; Fig. 2 and Table 1), comparable to other alkaline differentiated lavas from the Afar Rift in Ethiopia, Acension and Heard Islands (0.01–2.32‰; Fig. 2; Deng et al. 2019; Johnson et al. 2019; Zhao et al. 2020; Hoare et al. 2020). Our new Ti isotope data for the St. Helena samples confirm previous observations that alkaline differentiated lavas show the largest range in Ti isotope composition followed by tholeiitic and calc-alkaline magmas (Fig. 2; Millet et al. 2016; Greber et al. 2017a, 2021; Deng et al. 2019; Johnson et al. 2019, 2023; Zhao et al. 2020; Hoare et al. 2020). In addition, titanomagnetite separates from Group 3 samples have $\delta^{49/47}Ti$ values (−0.54 to 0.01‰) remarkably lower than the corresponding whole rock samples (from −0.02 to 0.21‰; Table 1) with $\Delta^{49/47}Ti_{Tmag\text{-}whole\ rock}$ ($= \delta^{49/47}Ti_{Tmag} - \delta^{49/47}Ti_{whole\ rock}$) values ranging from −0.68 to -0.22‰. This is consistent with previous investigations (Mandl 2019; Johnson et al. 2019, 2023; Greber et al. 2021; Rzehak et al. 2021, 2022; Hoare et al. 2022; Storck et al. 2023) and confirms the major control that Ti-oxide crystallization exerts on the Ti isotopic characteristics of igneous rocks.

The $\delta^{57/54}Fe$ values of sample SH-30 and sample SH-42 are summarized in Table S3 in Supporting Information S1. The $\delta^{57/54}Fe$ values range from 0.34 to 0.35‰, relatively higher than those previously measured in other Group 3 samples (0.17 to 0.32‰; Zhao et al. 2022).

Discussion

Our new results show significant Ti isotopic variability in St. Helena samples. Titanium is a moderately refractory element during igneous processes and a fluid immobile element (Pearce and Norry 1979; Kessel et al. 2005; Rapp et al. 2010), and thus Ti isotopic signatures are likely unaffected by processes such as low-temperature alteration. The Th/U ratios are commonly used as tracers for low-temperature alteration due to high mobility of U in oxidized geological fluids (Mathieu et al. 2001), while Th behaves as an immobile high field-strength element. U and Th are therefore often fractionated during low-temperature alteration. The absence of correlation between $\delta^{49/47}Ti$ and Th/U for St. Helena samples (Fig. 3a), further suggests that low-temperature alteration has an insignificant effect on $\delta^{49/47}Ti$ variation. Radiogenic isotope ratios, such as initial $^{87}Sr/^{86}Sr$ and $^{143}Nd/^{144}Nd$, are valuable tracers of source heterogeneity, however, no discernable correlation exists between $\delta^{49/47}Ti$ and initial $^{87}Sr/^{86}Sr_i$ (Fig. 3b) or $^{143}Nd/^{144}Nd$ (Fig. 3c) in St. Helena samples. This suggests source heterogeneity did not produce the measured Ti isotopic variability. Therefore, the large variation in $\delta^{49/47}Ti$ observed in St. Helena samples likely reflects isotopic fractionation during high temperature igneous processes. This will be more fully explored below, in light of the established fractional crystallization sequence (Wang et al. 2021; Zhao et al. 2022).

Ti isotopic fractionation during fractional crystallization

St. Helena Group 1 samples (MgO contents > 13 wt.%) have a limited range of Ti isotopic compositions ($\delta^{49/47}Ti$ = 0.03–0.04‰; Table 1 and Fig. 2), suggesting that olivine and clinopyroxene accumulation had a negligible influence on the Ti isotopic composition of the St. Helena lava. Group 2 samples also display a narrow $\delta^{49/47}Ti$ range (−0.02–0.05‰; Table 1), and show no discernable relationship between $\delta^{49/47}Ti$ and geochemical indicators of magma differentiation (e.g., SiO_2, MgO, TiO_2 and total-alkali contents; Fig. 2). This implies that fractional crystallization of olivine and clinopyroxene has little

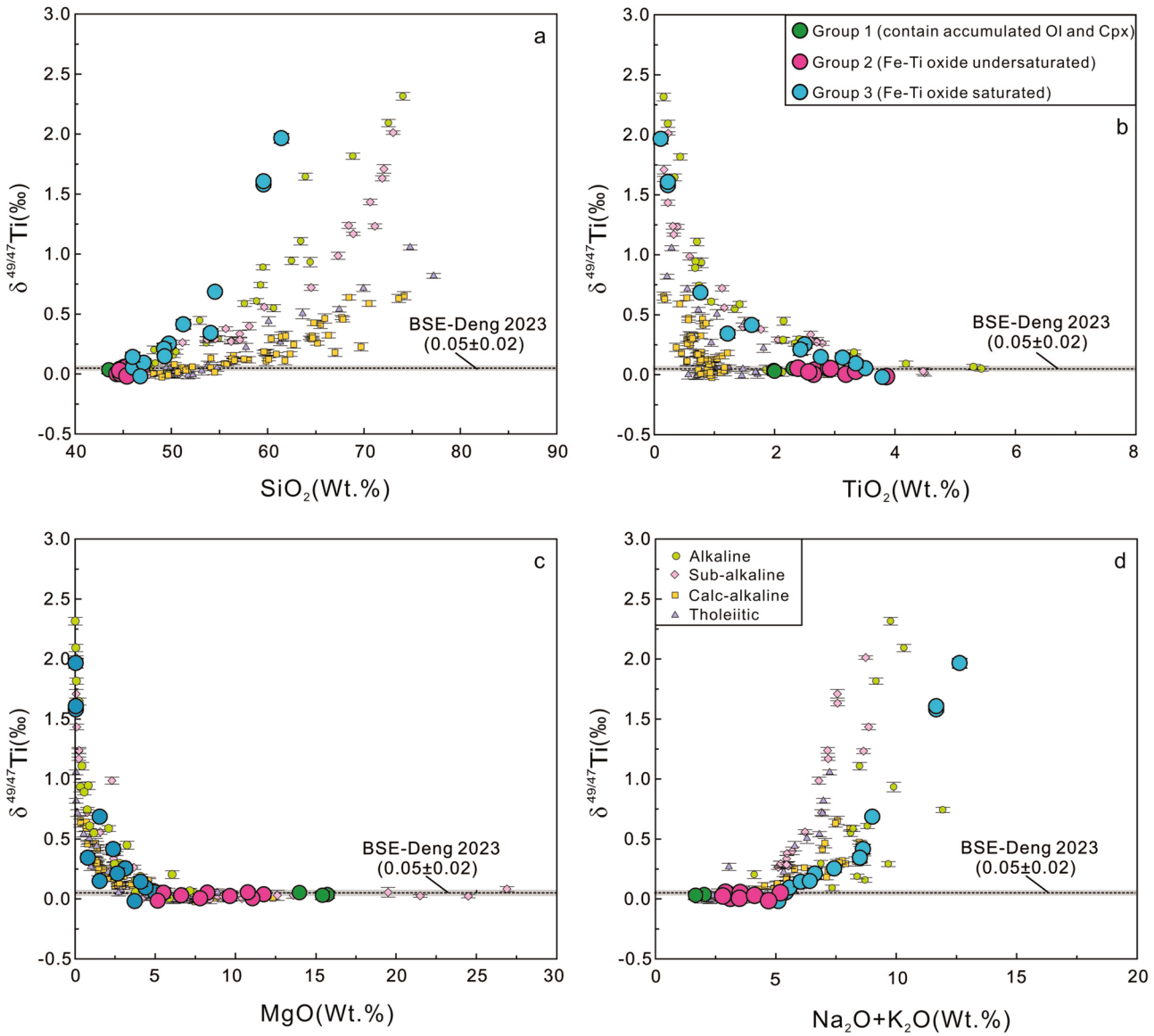

Fig. 2 Plot of $\delta^{49/47}$Ti vs SiO_2 (**a**), TiO_2 (**b**), MgO (**c**) and Na_2O+K_2O (**d**) contents for the studied St. Helena lavas. The horizontal line represents the average $\delta^{49/47}$Ti value of the bulk silicate Earth (BSE) (0.05 ± 0.02‰, 2SD; Deng et al. 2023). Also shown are literature data for alkaline (Ascension Island, Afar rift, Heard island; Hoare et al. 2020, 2022), subalkaline (Afar rift, Hekla in Iceland, Kilauea Iki; Deng et al. 2019; Johnson et al. 2019; Zhao et al. 2020), calc-alkaline (Santorini, Agung, Kos, Rindjani; Millet et al. 2016; Hoare et al. 2020, 2022; Greber et al. 2021; Johnson et al. 2023) and tholeiitic (Monowai seamount, Alarcon Rise, Koolau, Hawaii; Hoare et al. 2020, 2022; Zhao et al. 2020) rocks. Error bar denotes two standard deviation (2SD), with the exception of error bars from Millet et al. (2016), Johnson et al. (2019, 2023), Hoare et al. (2020, 2022) and Greber et al. (2021) which are 95% c.i.. The $\delta^{49/47}$Ti data for St. Helena samples are from Table 1

impact on the Ti isotopic composition of St. Helena lava. Titanium isotope fractionation during igneous processes is theoretically controlled by differences in bond stiffness and coordination number (CN) between mineral phases and the melt. A small CN and short bond favor incorporation of heavy isotopes at equilibrium (Urey 1947; Schauble 2004). Titanium is fourfold coordinated in olivine, and four to sixfold coordinated in silicate melt, depending on melt composition (average ~4.5 to 5.4, Farges and Brown 1997), olivine is therefore predicted to be slightly isotopically heavy relative to silicate melt (Wang et al. 2020). This prediction was confirmed by Greber et al. (2021) who found that olivine had a heavier Ti stable isotope composition than the bulk rock. However, fractional crystallization of olivine seems to have a negligible effect on the Ti isotope composition of St. Helena lavas due to its negligible TiO_2 contents. Unlike olivine, pyroxene can contain both six and fourfold coordinated Ti (Farges and Brown

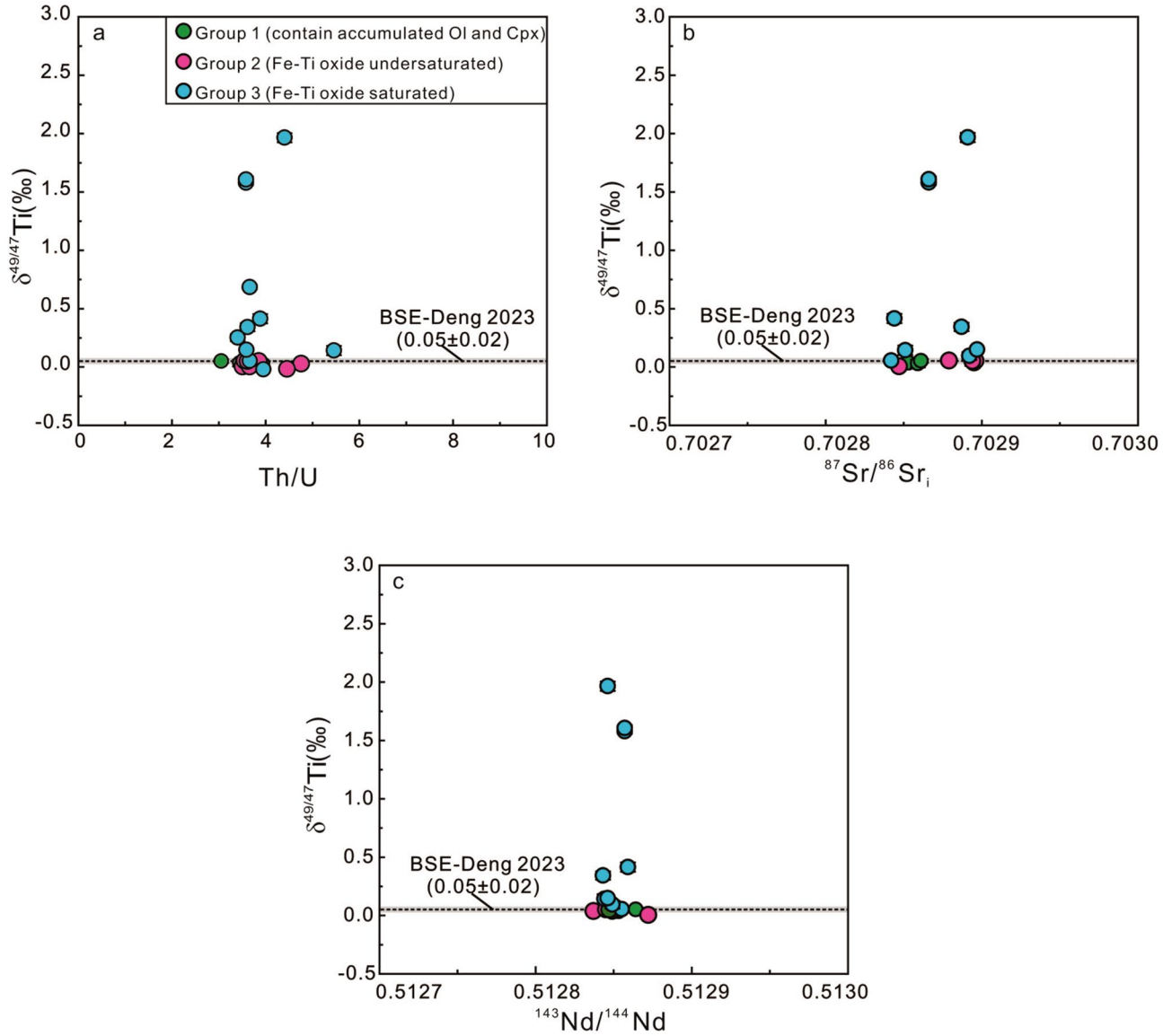

Fig. 3 $\delta^{49/47}$Ti versus Th/U (a), $^{87}Sr/^{86}Sr_i$ (b), and $^{143}Nd/^{144}Nd$ (**c**) for St. Helena samples analyzed in this study. The horizontal dashed line and shaded areas represent the average $\delta^{49/47}$Ti values of the BSE (0.05 ± 0.02‰, 2SD; Deng et al. 2023). Error bars are 2SD. $\delta^{49/47}$Ti data for St. Helena samples are from Table 1. The trace element and radiogenic isotope data are from Kawabata et al. (2011) and Hanyu et al. (2014), respectively, and can be found in Table S1 of Supporting Information S1

1997). Previous studies (Leitzke et al. 2018; Wang et al. 2020; Aarons et al. 2021) have indicated that if Ti is solely hosted in sixfold coordination in pyroxene, no discernable Ti isotopic fractionation would be expected between the pyroxene and the silicate melt. On the other hand, when Ti is exclusively hosted in fourfold coordination in pyroxene, pyroxene are isotopically heavier than the coexisting melt. In additon, Rzehak et al. (2021, 2022) demonstrated that pyroxene can produce resolvable Ti isotope fractionation under more reducing lunar conditions. Ti primarily occupies a sixfold coordination in pyroxene at upper mantle P–T conditions (Ackerson et al. 2017), and clinopyroxene is the main Ti-bearing phase in St. Helena Group 1 and Group 2 samples. The lack of resolvable Ti isotope variation in the St. Helena Group 1 and Group 2 samples supports the negligible impact of clinopyroxene-induced Ti isotopic fractionation.

In contrast, the St. Helena Group 3 samples (MgO content < 5.0 wt%) display a wide range in $\delta^{49/47}$Ti (− 0.02 to 1.96‰; Table 1 and Fig. 2) and clear correlation between $\delta^{49/47}$Ti and magma differentiation indicators such as SiO_2, MgO, TiO_2, and total-alkali contents (Fig. 2). As noted

above, Group 3 samples underwent massive fractionation of plagioclase and Fe-Ti oxide, with minor amounts of apatite, olivine, and clinopyroxene (Kawabata et al. 2011; Wang et al. 2021). Fractional crystallization of olivine and pyroxene had little effect on the Ti isotope variation in St. Helena Group1 and Group 2 samples according to our discussion above. Minerals like plagioclase and accessory apatite contain almost no TiO_2, so the effect of their crystallization is also limited. However, ulvöspinel-rich titanomagnetite is characterized by a high TiO_2 content (18.7–22.7 wt.%) and a remarkably lighter Ti isotopic composition ($\delta^{49/47}$Ti = -0.54 to 0.01‰) relative to the corresponding whole rock ($\delta^{49/47}$Ti = − 0.02 to 0.21‰; Table 1). When sufficient titanomagnetite crystallizes, it drives the evolved melt toward a heavier Ti isotopic composition and depletes the melt in TiO_2 and FeO_T, consistent with our observations (Fig. 1 and Fig. 2). This is because Fe-Ti oxides (such as titanomagnetite, rutile and ilmenite) exclusively host Ti in sixfold coordination (Leitzke et al. 2018; Wang et al. 2020; Aarons et al. 2021) and thus prefer light Ti isotopes relative to other silicate minerals and melts (Leitzke et al. 2018; Wang et al. 2020; Zhao et al. 2020; Aarons et al. 2021; Hoare et al. 2022). Consequently, the removal of Fe-Ti oxides would leave behind a residual magma isotopically heavy in Ti. This inference is supported by our newly measured and published Ti isotopic compositions of natural Fe-Ti oxide samples (Johnson et al. 2019, 2023; Mandl 2019; Aarons et al. 2021; Greber et al. 2021; Nie et al. 2021; Greber et al. 2021; Rzehak et al. 2021; Hoare et al. 2022), as well as experimental results (Rzehak et al. 2021, 2022; Hoare et al. 2022). Recent work by Wang et al. (2021) and Zhao et al. (2022) on the same samples from St. Helena have shown that Mg and Fe isotopic compositions of Group 3 samples vary and correlate with MgO contents, implying that these variations are largely controlled by ulvöspinel-rich titanomagnetite fractionation during magmatic differentiation. Most notably, the $\delta^{49/47}$Ti values of Group 3 samples negatively correlate with $\delta^{26/24}$Mg (Fig. 4a), and positively correlate with $\delta^{57/54}$Fe (Fig. 4b). We therefore conclude that ulvöspinel-rich titanomagnetite crystallisation was the dominant control on progressively heavier Ti isotope compositions in evolving St. Helena Group 3 samples.

Quantitative modeling

We modelled Ti isotopic fractionation during magma differention using the Rayleigh fractionation model described below:

$$\delta^{49/47}Ti_{melt} = (\delta^{49/47}Ti_{initialmelt} + 1000) \times f_{Ti}^{(a-1)} - 1000$$

where a ($(^{49}Ti/^{47}Ti)_{mineral}$ /$(^{49}Ti/^{47}Ti)_{melt}$)) is the Ti isotope fractionation factor between mineral and melt, and f_{Ti} is the mass fraction of Ti in the remaining melt. f_{Ti} is estimated by comparing the Ti/Th ratios of the samples, assuming a partition coefficient of zero between mineral and melt for Th. In

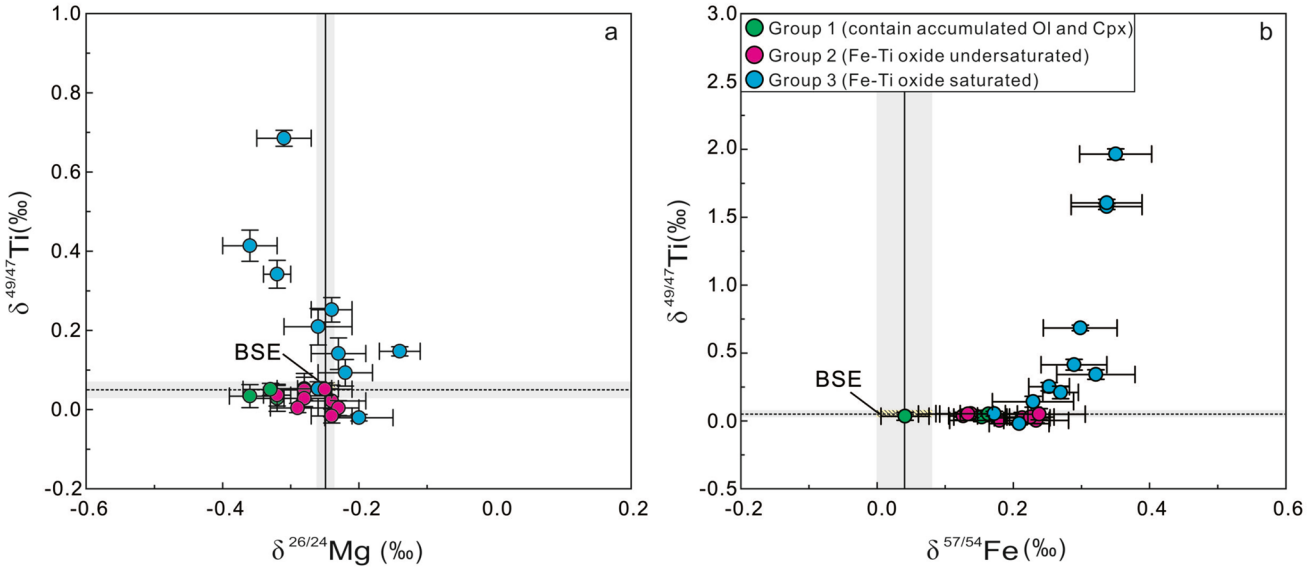

Fig. 4 $\delta^{49/47}$Ti versus $\delta^{26/24}$Mg (**a**) and $\delta^{57/54}$Fe (**b**) for St. Helena lavas. The horizontal dashed line denotes the average $\delta^{49/47}$Ti value of the BSE (0.05 ± 0.02‰, 2SD; Deng et al. 2023). The vertical solid line in panel (**a**) represents the average $\delta^{26/24}$Mg of the BSE (− 0.25 ± 0.04‰, Teng et al. 2017), and the vertical solid line in panel (b) represents the upper mantle Fe isotopic composition ($\delta^{57/54}$Fe = 0.04 ± 0.04‰, Weyer and Ionov 2007; Craddock et al. 2013). $\delta^{49/47}$Ti data for St. Helena samples are from Table 1. Error bars are 2SD. $\delta^{57/54}$Fe data for samples SH-30 and SH-42 are from Table S3 of Supporting Information S1. Literature Mg and Fe isotope data are taken from Wang et al. (2021) and Zhao et al. (2022), respectively, and can be found in Table S1 of Supporting Information S1

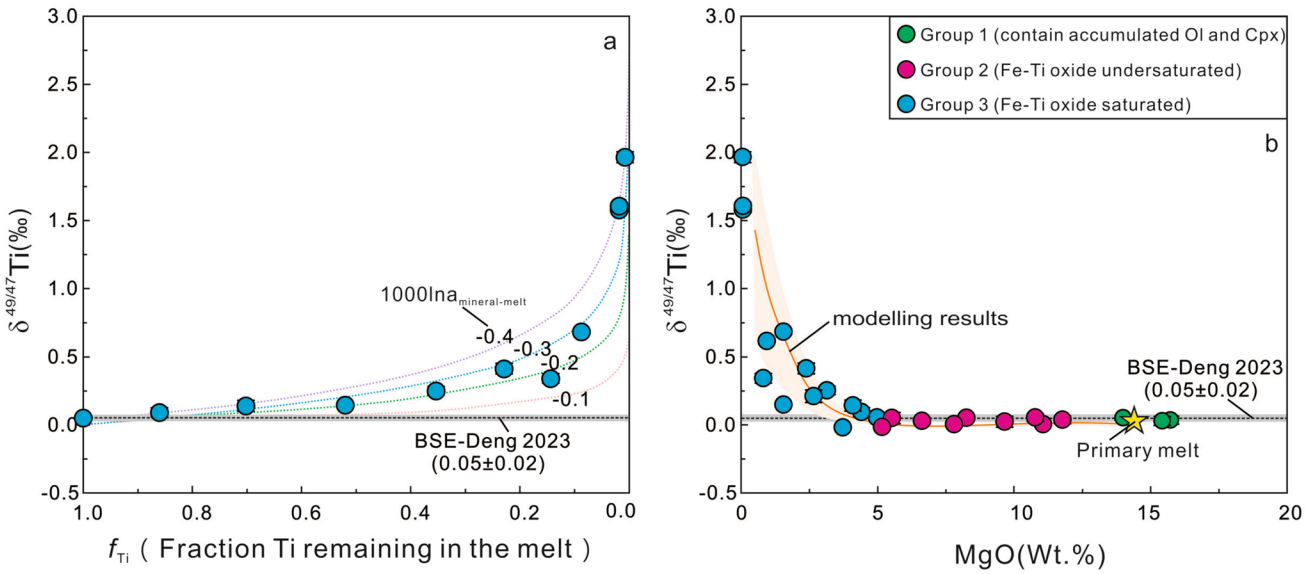

Fig. 5 Comparison of Ti isotope composition of samples from the St. Helena with a Rayleigh fractionation model using different bulk isotope fraction factors (1000 $\ln\alpha_{\text{mineral-melt}}$) between all crystallizing minerals and the silicate melt (see Table S4 of Supporting Information S1 for details) (**a**). Plot of $\delta^{49/47}$Ti vs MgO contents for the studied St. Helena lavas (see Table S5 of Supporting Information S1 for details of quantitative modelling) (**b**). The light orange shaded area represents the uncertainty of the calculated $\delta^{49/47}$Ti variation that derives from the uncertainty of the titanomagnetite-melt isotopic fractionation factor ($\Delta^{49/47}\text{Ti}_{\text{Tmag-melt}} = [(-0.058 \pm 0.015)*\text{TiO}_2 + (0.15 \pm 0.24)] \times 10^6/\text{T}^2$) from Johnson et al. (2023). The major element data of primary melt is from Kawabata et al. (2011) and the $\delta^{49/47}$Ti value of primary melt is assumed as 0.00‰. The horizontal dashed line and shaded areas represents the average $\delta^{49/47}$Ti values of BSE (0.05 ± 0.02‰, 2SD; Deng et al. 2023). $\delta^{49/47}$Ti data for St. Helena samples are from Table 1. Error bars are 2SD. Major element data for the studied samples are from Kawabata et al. (2011)

our simulation, sample SH-58 ($\delta^{49/47}\text{Ti} = 0.05$‰), with the highest MgO (4.97 wt%) and TiO_2 (3.51 wt%) was chosen as the initial melt composition, with MgO ≈ 5 wt.% marking the onset of Fe-Ti oxide saturation (Kawabata et al. 2011; Wang et al. 2021; Zhao et al. 2022). Figure 5a shows that the f_{Ti} vs. $\delta^{49/47}$Ti trend of St. Helena Group 3 samples can be reconciled by $\Delta^{49/47}\text{Ti}_{\text{mineral-melt}}$ ($= 1000\ln a^{49/47}\text{Ti}_{\text{mineral-melt}}$) of −0.40 to −0.30‰ (see Table S4 in Supporting Information S1 for details of quantitative modelling).

To further assess the impact of titanomagnetite crystallization on Ti isotopic composition of St. Helena lavas, we modelled Ti isotopic fractionation following the modelling method of Wang et al. (2021) and Zhao et al. (2022), who quantitatively evaluated the effect of each separated mineral on the Mg and Fe isotopic compositions of St. Helena lavas, respectively. An isotope mass balance model is used to calculate the Ti isotopic composition of residual melts after each crystallization step, and it can be expressed as the following equations:

$$\delta^{49/47}Ti_{melt,1} = \frac{\delta^{49/47}Ti_{melt,2} \times f_{melt,2} \times TiO_{2melt,2} + \sum_{i=1}^{n} \delta^{49/47}Ti_i \times f_{i,2} \times TiO_{2i,2}}{\left(f_{melt,2} \times TiO_{2melt,2} + \sum_{i=1}^{n} f_{i,2} \times TiO_{2i,2}\right)} \quad (1)$$

$$\delta^{49/47}Ti_i = \Delta^{49/47}Ti_{i-melt} + \delta^{49/47}Ti_{melt,2} \quad (2)$$

where $\delta^{49/47}\text{Ti}_{\text{melt, 1}}$ and $\delta^{49/47}\text{Ti}_{\text{melt, 2}}$ are the Ti isotopic compositions of the melts before and after a crystallization step, respectively. $\delta^{49/47}\text{Ti}_i$ is the Ti isotopic composition of mineral i, and $\Delta^{49/47}\text{Ti}_{i\text{-melt}}$ is the Ti isotopic fractionation between mineral i and melt. $TiO_{2melt,2}$ and $TiO_{2i,2}$ denote the TiO_2 contents of residual melts and separated mineral i after a crystallization step, respectively. The proportions of segregated mineral i and residual melts after each crystallization step are marked as $f_{i,\,2}$ and $f_{\text{melt, 2}}$, respectively. Olivine, clinopyroxene, and titanomagnetite are used in the modeling calculations. Apatite and plagioclase are ignored in our modeling calculations due to their very low TiO_2 contents. The chemical compositions and proportions of segregated minerals and residual melts during the evolution history of St. Helena samples are from published MELTS calculation results (Table S5 in Supporting Information S1; Wang et al. 2021). The melt-mineral isotope fractionation between melts and silicate minerals such as olivine and clinopyroxene is assumed to be zero, and the titanomagnetite-melt isotopic fractionation factor is from Johnson et al. (2023). The modeling results are reported in Table S5 in

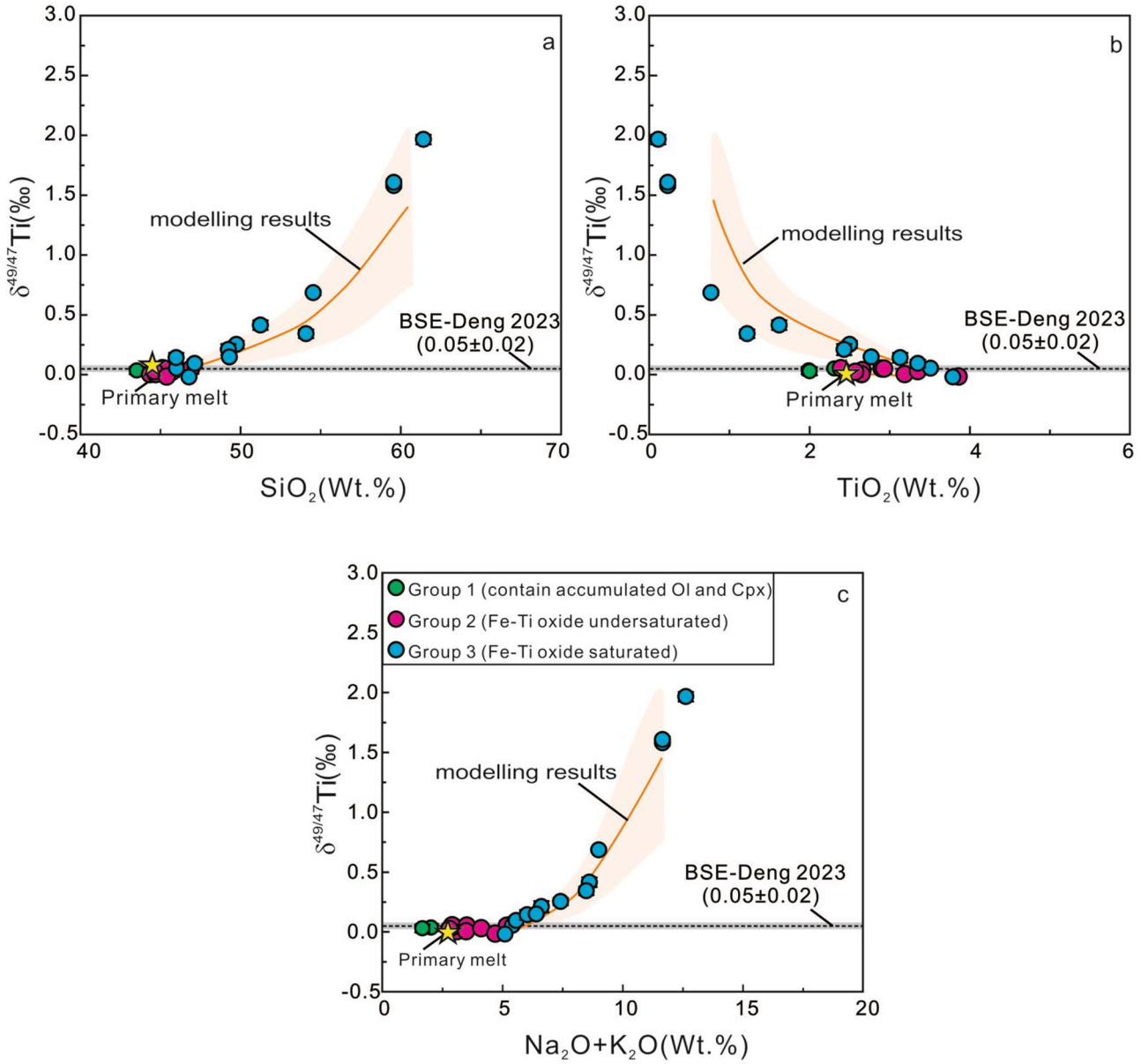

Fig. 6 Plot of $\delta^{49/47}$Ti vs SiO_2 (a), TiO_2 (b), and Na_2O+K_2O (**c**) contents for the studied St. Helena lavas. The orange lines show the modeled variation of $\delta^{49/47}$Ti with changing SiO_2, TiO_2, and Na_2O+K_2O contents (see Table S5 of Supporting Information S1 for details of quantitative modelling). The light orange shaded area represents the uncertainty of the calculated $\delta^{49/47}$Ti variation that derives from the uncertainty of the titanomagnetite-melt isotopic fractionation factor ($\Delta^{49/47}Ti_{Tmag\text{-}melt}=[(-0.058\pm0.015)*TiO_2+(0.15\pm0.24)]\times10^6/T^2$; Johnson et al. 2023). The major element data of primary melt is from Kawabata et al. (2011) and the $\delta^{49/47}$Ti value of primary melt is assumed as 0.00‰. The horizontal dashed line and shaded areas represents the average $\delta^{49/47}$Ti values of BSE (0.05 ± 0.02‰, 2SD; Deng et al. 2023). $\delta^{49/47}$Ti data for St. Helena samples are from Table 1. Error bars are 2SD. Major element data for the studied samples are from Kawabata et al. (2011)

Supporting Information S1 and illustrated in Fig. 5b and Fig. 6. As shown in Fig. 5b, the measured trend of $\delta^{49/47}$Ti versus MgO for St. Helena samples can be well modeled using the above method. Furthermore, the observed trends of $\delta^{49/47}$Ti versus SiO_2, TiO_2 and total-alkali contents can be modeled for most St. Helena samples except for the two most evolved sample (e.g., SH-30, SH-42) with extremely low MgO (0.05–0.06 wt.%) and TiO_2 (0.11–0.23 wt.%) contents (Table 1 and Fig. 6). This discrepancy is probably due to the fact that the MELTS calculations failed to perfectly reproduce the true modes of Fe-Ti oxide minerals and especially the accurate MgO and TiO_2 contents of the residual melt and Fe-Ti oxides near the end of magma differentiation at St. Helena (Wang et al. 2021). Nonetheless,

our modelling results reaffirm that titanomagnetite crystallization is the major control on the progressive elevation of $\delta^{49/47}$Ti observed in St. Helena Group 3 samples.

Comparison with previous studies

Several studies have shown that differentiated lavas (alkaline, tholeiitic and calc-alkaline series) experience different Ti isotopic evolution pathways during magmatic evolution (Deng et al. 2019; Johnson et al. 2019, 2023; Hoare et al. 2020, 2022; Zhao et al. 2020). New Ti isotopic analyses for the St. Helena samples confirm this conclusion (Fig. 2). For example, at a given SiO_2 content, the St. Helena Group 3 samples and other alkaline magmas show a greater increase in $\delta^{49/47}$Ti (−0.04 to 2.32‰; Deng et al. 2019; Johnson et al. 2019; Hoare et al. 2020; Zhao et al. 2020) than tholeiitic (0.01 to 1.06‰; Zhao et al. 2020; Hoare et al. 2020, 2022) and calc-alkaline (0.04 to 0.65‰; Millet et al. 2016; Greber et al. 2021; Hoare et al. 2020; 2022; Johnson et al. 2023) magma series (Fig. 2a). These differences likely result from caused by crystallization of a range of Fe-Ti oxides (e.g., magnetite, ilmenite, and pseudobrookite) with contrasting Ti isotopic compositions throughout magma evolution (Deng et al. 2019; Johnson et al. 2019, 2023; Hoare et al. 2020, 2022; Zhao et al. 2020). Both theoretical models and measurement of rock samples have demostrated that titanomagnetite is highly enriched in isotopically light Ti relative to other Fe-Ti oxides (ilmenite, rutile, and pseudobrookite) at equilibrium (Johnson et al. 2019, 2023; Wang et al. 2020; Zhao et al. 2020; Hoare et al. 2020, 2022; Greber et al. 2021). Therefore, at magmatic temperatures, progressive crystallization of titanomagnetite-dominanted Fe-Ti oxide raises the melt $\delta^{49/47}$Ti values more than crystallization of other Fe-Ti oxides (ilmenite, rutile, and pseudobrookite). Both Ti^{4+} and Fe^{2+} occupy the six-fold site in titanomagnetite. Given that the Fe^{2+} ion is larger than Ti^{4+}, titanomagnetite has a relatively longer Ti–O bond length (2.05–2.06 Å) than other Fe-Ti oxides such as ilmenite, rutile, and pseudobrookite (1.94–1.99 Å) (Smyth and Bish 1988; Howard et al. 1991; Farges et al. 1996a, b; Bosi et al. 2009). This longer Ti–O bond length means that light Ti is preferentially accommodated in the titanomagnetite structure at equilibrium (Bigeleisen and Mayer 1947; Urey 1947; Schauble 2004). Our results show that the St. Helena Group 3 samples display higher $\delta^{49/47}$Ti than other alkaline differentiated lavas at a given SiO_2 from the Afar Rift in Ethiopia, Acension and Heard Islands (Fig. 2; Deng et al. 2019; Johnson et al. 2019; Zhao et al. 2020; Hoare et al. 2020). As discussed above, magmas that crystallize various Fe-Ti oxides (such as titanomagnetite, rutile and ilmenite) with divergent Ti isotopic compositions will preserve distinct Ti isotope compositions. At St. Helena, ulvöspinel-rich titanomagnetite is the only crystallization Fe-Ti oxide phase during the compositional range of our studied Group 3 samples (Fe-Ti oxide saturated), whereas both titanomagnetite and ilmenite are Ti-bearing crystallization phases in other alkaline differentiated lavas. Ulvöspinel-rich titanomagnetite is expected to have much lower $\delta^{49/47}$Ti than other Fe-Ti oxides (e.g., Hoare et al. 2020, 2023; Johnson et al. 2023). The difference between St. Helena Group 3 samples and other alkaline differentiated lavas is probably due to an earlier saturation and higher extent of ulvöspinel-rich titanomagnetite crystallization from St. Helena Group 3 samples compared to other alkaline differentiated lavas.

Another factor controlling Ti isotopic fractionation is the composition of crystallising titanomagnetite. For example, the TiO_2 content (15.9–28 wt.%) of titanomagnetite crystallized from alkaline/sub-alkaline lavas in intraplate settings (Afar, Ascension, Kilauea, Hekla, Heard; Deng et al. 2019; Johnson et al. 2019; Zhao et al. 2020; Hoare et al. 2020, 2022) is significantly higher than that of titanomagnetite crystallized from arc-related calc-alkaline lavas (TiO_2 = 7–13.0 wt.%; Hailar, Kos Agung, Santorini, Rindjani; Millet et al. 2016; Hoare et al. 2020, 2022; Zhao et al. 2020; Greber et al. 2021; Johnson et al. 2023). This compositional contrast likely explains the difference in the Ti isotopic evolution path of rocks in these two settings (Fig. 2). This speculation is supported by Hoare et al. (2022) who observed that Ti–rich titanomagnetite (~ 22 wt.%, TiO_2) was isotopically lighter than Ti-poor magnetite (~ 14 wt% TiO_2). This is also evidenced by a subsequent study by Johnson et al. (2023) who observed that Rindjani Ti-poor calc-alkaline lavas crystallizing Ti-poor magnetite (7–10 wt%, TiO_2) experienced less Ti isotopic fractionation compared to other magma series. Further corroboration comes from the results produced in this work where the dominant Fe-Ti oxide in the St. Helena Group 3 samples is TiO_2 enriched ulvöspinel-rich titanomagnetite (18.7–22.7 wt.% TiO_2; Wang et al. 2021; Zhao et al. 2022) with a remarkably light Ti isotopic composition ($\delta^{49/47}$Ti = − 0.54–0.01‰; Table 1). The diverse Ti isotope fractionation trends observed in various magmatic systems is indirectly governed by the parental melt chemistry and redox state, which could control the onset of Fe-Ti oxide crystallizaion, as well as its modal abudance and compostition (Deng et al. 2019; Zhao et al. 2020; Hoare et al. 2020, 2022). For example, alkaline magmas from intraplate settings (reduced and H_2O-poor) have higher initial melt TiO_2 contents than those of tholeiitic and calc-alkaline lavas (oxidized and H_2O-rich; Prytulak and Elliot 2007), which enables early saturation of Ti–rich titanomagnetite or ilmenite with high modal abundance (Hoare et al. 2020, 2022). This will also drive larger Ti fractionation in alkaline magmas relative to tholeiitic and calc-alkaline arc lavas with lower TiO_2 contents and less Fe-Ti oxide (Deng et al. 2019; Zhao et al. 2020; Hoare et al. 2020, 2022). Additionally, recent studies by Storck et al. (2023) and Johnson et al.

(2023) have demonstrated that the relative Ti fractions in crystallized minerals (silicate minerals such as amphibole or pyroxene vs. Fe-Ti oxides) can also influence Ti stable isotope fractionation in magmatic systems. As outlined in Johnson et al. (2023), this effect might be an indirect result of the elevated Fe^{3+}/Fe^{2+} ratio in calc-alkaline systems.

Conclusions

This study explores the Ti isotope fractionation behavior during the differentiation of St Helena alkaline magma. Important conclusions include:

(1) The $\delta^{49/47}$Ti range of St. Helena Group 1 and Group 2 samples (MgO > 5 wt.%) is quite narrow (−0.02 to 0.05‰). The absence of systematic correlations between $\delta^{49/47}$Ti and the chemical indicators of magmatic differentiation (e.g., SiO_2, MgO, TiO_2 and $Na_2O + K_2O$ contents) indicate that accumulation or crystallization of olivine and clinopyroxene have negligible influence of the $\delta^{49/47}$Ti variation of St. Helena Group 1 and Group 2 samples.

(2) Significant Ti isotopic variations ($\delta^{49/47}$Ti = −0.02 to 1.96‰) are observed for St. Helena Group 3 samples (MgO < 5 wt.%), and there are clear correlations between $\delta^{49/47}$Ti and SiO_2, MgO, TiO_2 and total-alkali contents, which are the result of fractional crystallization of isotopically light ulvöspinel-rich titanomagnetite. This is reinforced by the measured lower $\delta^{49/47}$Ti values for ulvöspinel-rich titanomagnetite relative to whole rock ($\Delta^{49/47}Ti_{Tmag\text{-}whole\ rock} = -0.68$ to −0.22‰) of the St. Helena Group 3 samples. Quantitative geochemical modeling also support crystallization and removal of isotopically light ulvöspinel-rich titanomagnetite resulting in isotopically heavy St. Helena Group 3 samples.

(3) Our study further confirms that the Ti isotopic fractionation trends observed in different magmatic systems (alkaline, tholeiitic and calc-alkaline series) could be the result of crystallization of different Fe-Ti oxides (Titanomagnetite, ilmenite, magnetite) with distinct light Ti isotopic compositions depending on the different melt TiO_2 composition, oxygen fugacity and water activity.

Supplementary Information The online version contains supplementary material available at https://doi.org/10.1007/s00410-023-02085-x.

Acknowledgements This project was funded by the National Natural Science Foundation of China (42122020 and 41973015) and the National Key R&D Program of China (2019YFA0708400). We appreciate Nicolas Dauphas and Zhengbin Deng for providing the OL-Ti and IGPG-Ti standards. We are also grateful to Zhiyong Zhu and Jianxiong Ma for Ti isotope analyses. We warmly thank the editor Othmar Müntener and anonymous reviewers for their constructive comments and suggestions.

Data availability Data relating to this work are available in the main text or Supplementary Information.

Declarations

Conflict of Interest The authors declare that they have no known conflicts of interest.

References

Aarons SM, Reimink JR, Greber ND, Heard AW, Zhang Z, Dauphas N (2020) Titanium isotopes constrain a magmatic transition at the Hadean-Archean boundary in the Acasta Gneiss Complex. Sci Adv 6:1–9

Aarons SM, Dauphas N, Blanchard M, Zeng H, Nie NX, Johnson AC, Greber ND, Hopp T (2021) Clues from ab initio calculations on titanium isotopic fractionation in tholeiitic and calc-alkaline magma series. ACS Earth Space Chem 5:2466–2480

Ackerson MR, Tailby ND, Watson EB (2017) XAFS spectroscopic study of Ti coordination in garnet. Am Mineral 102:173–183

An YJ, Huang JX, Griffin WL, Liu CZ, Huang F (2017) Isotopic composition of Mg and Fe in garnet peridotites from the Kaapvaal and Siberian cratons. Geochim Cosmochim Acta 200:167–185

Anguelova M, Fehr MA, Takazawa E, Schönbächler M (2022) Titanium isotope heterogeneity in the Earth's mantle: a case study of the Horoman peridotite massif. Geochim Cosmochim Acta 355:356–368

Baker I (1968) Intermediate oceanic volcanic rocks and the 'Daly gap.' Earth Planet Sci Lett 4:103–106

Baker I (1969) Petrology of the volcanic rocks of Saint Helena Island. South Atlantic Geol Soc Am Bull 80:1283

Bigeleisen J, Mayer MG (1947) Calculation of equilibrium constants for isotopic exchange reactions. J Chem Phys 15:261–267

Bosi F, Halenius U, Skogby H (2009) Crystal chemistry of the magnetite-ulvospinel series. Am Miner 94:181–189

Chaffey DJ, Cliff RA, Wilson BM (1989) Characterization of the St. Helena magma source. Geol Soc (Lond) Spec Publ 42: 257–276.

Chen KY, Bao ZA, Yuan HL, Lv N (2022) Direct measurement of Fe isotope compositions in iron-dominated minerals without column chromatography using MC-ICP-MS. J Anal at Spectrom 37(2):249–263

Craddock PR, Dauphas N (2011) Iron isotopic compositions of geological reference materials and chondrites. Geostand Geoanal Res 35:101–123

Craddock PR, Warren JM, Dauphas N (2013) Abyssal peridotites reveal the near-chondritic Fe isotopic composition of the Earth. Earth Planet Sci Lett 365:63–76

Deng ZB, Moynier F, Sossi PA, Chaussidon M (2018a) Bridging the depleted MORB mantle and the continental crust using titanium isotopes. Geochem Perspect Lett 1:53–64

Deng ZB, Moynier F, van ZuilenK SPA, Pringle EA, Chaussidon M (2018b) of resolvable titanium stable isotopic variations in bulk chondrites. Geochim Cosmochim Acta 239:409–419

Deng ZB, Chaussidon M, Savage P, Robert F, Pik R, Moynier F (2019) Titanium isotopes as a tracer for the plume or island arc affinity of felsic rocks. Proc Natl Acad Sci USA 116:1132–1135

Deng ZB, Schiller M, Jackson MG, Millet MA, Pan L, Nikolajsen K, Saji NS, Huang DY, Bizzarro M (2023) Earth's evolving geodynamic regime recorded by titanium isotopes. Nature 621:100–104

Farges F, Brown GE (1997) Coordination chemistry of titanium (IV) in silicate glasses and melts: IV. XANES studies of synthetic and natural volcanic glasses and tektites at ambient temperature and pressure. Geochim Cosmochim Acta 61:1863–1870

Farges F, Brown GE, Navrotsky A, Gan H, Rehr JJ (1996a) Coordination chemistry of Ti (IV) in silicate glasses and melts: II. Glasses at ambient temperature and pressure. Geochim Cosmochim Acta 60:3039–3053

Farges F, Brown GE Jr, Rehr JJ (1996b) Coordination chemistry of Ti(IV) in silicate glasses and melts: I. XAFS study of titanium coordination in oxide compounds. Geochim Cosmochim Acta 60:3023–3038

Greber ND, Dauphas N, Bekker A, Ptáček MP, Bindeman IN, Hofmann A (2017a) Titanium isotopic evidence for felsic crust and plate tectonics 3.5 billion years ago. Science 357:1271–1274

Greber ND, Dauphas N, Puchtel IS, Hofmann BA, Arndt NT (2017b) Titanium stable isotopic variations in chondrites, achondrites and lunar rocks. Geochim Cosmochim Acta 213:534–552

Greber ND, Pettke T, Vilela N, Lanari P, Dauphas N (2021) Titanium isotopic compositions of bulk rocks and mineral separates from the Kos magmatic suite: Insights into fractional crystallization and magma mixing processes. Chem Geol 578:120303

Hanyu T, Kawabata H, Tatsumi Y, Kimura JI, Hyodo H, Sato K, Miyazaki T, Chang Q, Hirahara Y, Takahashi T, Senda R, Nakai S (2014) Isotope evolution in the HIMU reservoir beneath St. Helena: implications for the mantle recycling of U and Th. Geochim Cosmochim Acta 143:232–252

He YS, Ke S, Teng FZ, Wang TT, Wu HJ, Lu YH, Li SG (2015) High-precision iron isotope analysis of geological reference materials by high-resolution MC-ICP-MS. Geostand Geoanal Res 39:341–356

He XY, Ma JL, Wei GJ, Zhang L, Wang ZB, Wang QS (2020) A new procedure for titanium separation in geological samples for $^{49}Ti/^{47}Ti$ ratio measurement by MC-ICP-MS. J Anal at Spectrom 35:100–106

Hoare L, Klaver M, Saji NS, Gillies J, Parkinson IJ, Lissenberg CJ, Millet MA (2020) Melt chemistry and redox conditions control titanium isotope fractionation during magmatic differentiation. Geochim Cosmochim Acta 282:38–54

Hoare L, Klaver M, Muir DD, Klemme S, Barling J, Parkinson IJ, Millet MA (2022) Empirical and experimental constraints on Fe-Ti oxide-melt titanium isotope fractionation factors. Geochim Cosmochim Acta 326:253–272

Howard CJ, Sabine TM, Dickson F (1991) Structural and thermal parameters for rutile and anatase. Acta Crystallogr B 47:462–468

Johnson AC, Aarons SM, Dauphas N, Nie NX, Zeng H, Helz RT, Romaniello SJ, Anbar AD (2019) Titanium isotopic fractionation in Kilauea Iki lava lake driven by oxide crystallization. Geochim Cosmochim Acta 264:180–190

Johnson AC, Zhang ZJ, Dauphas N, Rudnick RL, Foden J, Toc M (2023) Redox and mineral controls on Fe and Ti isotopic fractionations during calc-alkaline magmatic differentiation. Geochim Cosmochim Acta 355:1–12

Kawabata H, Hanyu T, Chang Q, Kimura JI, Nichols ARL, Tatsumi Y (2011) The petrology and geochemistry of St. Helena Alkali Basalts: evaluation of the oceanic crust-recycling model for HIMU OIB. J Petrol 52:791–838

Kessel R, Schmidt MW, Ulmer P, Pettke, (2005) Trace element signature of subduction-zone fluids, melts and supercritical liquids at 120–180 km depth. Nature 437(7059):724–727

Klemme S, Günther D, Hametner K, Prowatke S, Zack T (2006) The partitioning of trace elements between ilmenite, ulvospinel, armalcolite and silicate melts with implications for the early differentiation of the moon. Chem Geol 234(3–4):251–263

Kommescher S, Fonseca R, Kurzweil F, Thiemens M, Münker C, Sprung P (2020) Unravelling lunar mantle source processes via the Ti isotope composition of lunar basalts. Geochem Perspect Lett 13:13–18

Konter JG, Pietruszka AJ, Hanan BB, Finlayson VA, Craddock PR, Jackson MG, Dauphas N (2016) Unusual $\delta^{56}Fe$ values in Samoan rejuvenated lavas generated in the mantle. Earth Planet Sci Lett 450:221–232

Leitzke FP, Fonseca ROC, Göttlicher J, Steininger R, Jahn S, Prescher C, Lagos M (2018) Ti K-edge XANES study on the coordination number and oxidation state of Titanium in pyroxene, olivine, armalcolite, ilmenite, and silicate glass during mare basalt petrogenesis. Contrib Mineral Petrol 173:1–17

Li J, Tang SH, Zhu XK, Ma JX, Zhao XM (2022) Titanium isotope analysis of igneous reference materials using a Double-Spike MC-ICP-MS method. Acta Geol Sin 96(2):517–524

Mandl MB (2019) Titanium isotope fractionation on the Earth and Moon: constraints on magmatic processes and moon formation. Dissertation, ETH Zurich. https://doi.org/10.3929/ethz-b-000351171

Mathieu R, Zetterström L, Cuney M, Gauthier-Lafaye F, Hidaka H (2001) Alteration of monazite and zircon and lead migration as geochemical tracers of fluid paleocirculations around the Oklo-Okélobondo and Bangombé natural nuclear reactor zones (Franceville basin, Gabon). Chem Geol 171:147–171

Millet MA, Dauphas N (2014) Ultra-precise titanium stable isotope measurements by double-spike high resolution MC-ICP-MS. J Anal at Spectrom 29:1444–1458

Millet MA, Dauphas N, Greber ND, Burton KW, Dale CW, Debret B, Macpherson CG, Nowell GM, Williams HM (2016) Titanium stable isotope investigation of magmatic processes on the Earth and Moon. Earth Planet Sci Lett 449:197–205

Pearce JA, Norry MJ (1979) Petrogenetic implications of Ti, Zr, Y, and Nb variations in volcanic rocks. Contrib Mineral Petrol 69(1):33–47

Prytulak J, Elliott T (2007) TiO_2 enrichment in ocean island basalts. Earth Planet Sci Lett 263:388–403

Rapp JF, Klemme S, Butler IB, Harley SL (2010) Extremely high solubility of rutile in chloride and fluoride-bearing metamorphic fluids: an experimental investigation. Geology 38(4):323–326

Rzehak LJA, Kommescher S, Kurzweil F, Sprung P, Leitzke FP, Fonseca ROC (2021) The redox dependence of titanium isotope fractionation in synthetic Ti-rich lunar melts. Contrib Mineral Petrol 176:1–16

Rzehak LJA, Kommescher S, Hoare L, Kurzweil F, Sprung P, Leitzke F, Fonseca R (2022) Redox-dependent Ti stable isotope fractionation on the Moon: implications for current lunar magma ocean models. Contrib Mineral Petrol 177:81

Schauble EA (2004) Applying stable isotope fractionation theory to new systems. Rev Mineral Geochem 55:65–111

Smyth JR, Bish L (1988) Crystal structure and cation sites of the rock forming minerals. Allen and Unwin, Boston

Sossi PA, Foden JD, Halverson GP (2012) Redox-controlled iron isotope fractionation during magmatic differentiation: an example from the Red Hill intrusion. S Tasmania Contrib Mineral Petrol 164:757–772

Storck JC, Greber ND, Duarte JFV, Lanari P, Tiepolo M, Pettke T (2023) Molybdenum and titanium isotopic signatures of arc-derived cumulates. Chem Geol 617:121260

Teng FZ (2017) Magnesium isotope geochemistry. Rev Mineral. Geochemistry 82:219–287

Urey HC (1947) The thermodynamic properties of isotopic substances. J Chem Soc. https://doi.org/10.1039/jr9470000562

Wang WZ, Huang SC, Huang F, Zhao XM, Wu ZQ (2020) Equilibrium inter-mineral titanium isotope fractionation: Implication for high-temperature titanium isotope geochemistry. Geochim Cosmochim Acta 269:540–553

Wang XJ, Chen LH, Hanyu T, Zhong Y, Shi JH, Liu XW, Kawabata H, Zeng XLW (2021) Magnesium isotopic fractionation during basalt differentiation as recorded by evolved magmas. Earth Planet Sci Lett 565:116954

Weyer S, Ionov DA (2007) Partial melting and melt percolation in the mantle: the message from Fe isotopes. Earth Planet Sci Lett 259:119–133

Williams NH, Fehr MA, Parkinson IJ, Mandl MB, Schönbächler M (2021) Titanium isotope fractionation in solar system materials. Chem Geol 568:120009

Zhang XY, Chen LH, Wang XJ, Hanyu T, Hofmann AW, Komiya T, Nakamura K, Kato Y, Zeng G, Gou WX, Li WQ (2022) Zinc isotopic evidence for recycled carbonate in the deep mantle. Nat Commun 13:6085

Zhao XM, Zhang HF, Zhu XK, Tang SH, Yan B (2012) Iron isotope evidence for multistage melt–peridotite interactions in the lithospheric mantle of eastern China. Chem Geol 292–293:127–139

Zhao XM, Tang SH, Li J, Wang H, Helz R, Marsh B, Zhu XK, Zhang HF (2020) Titanium isotopic fractionation during magmatic differentiation. Contrib Mineral Petrol 175:1–16

Zhao J, Wang XJ, Chen LH, Hanyu T, Shi JH, Liu XW (2022) The effect of Fe-Ti oxide separation on iron isotopic fractionation during basalt differentiation. Contrib Mineral Petrol 177(10):101